mater.scichina.com link.springer.com

Sci China Mater 2025, 68(10): 3591–3599
https://doi.org/10.1007/s40843-025-3555-y

Dual-mode photochromic luminescence of carbon dots induced by photoinduced electron transfer

Jueran Cao, Enlin Huang, Ziting Zhong, Tingjie Jiang, Haoran Zhang, Wei Li, Xuejie Zhang, Chaofan Hu* and Bingfu Lei*

ABSTRACT **The integration of photochromism and photoluminescence in functional materials presents significant challenges, particularly in achieving broad-spectrum color modulation and rapid response. In this work, we have developed sodium-doped and sodium/boron co-doped CDs that exhibit dual-mode photochromic luminescent behavior through a novel radical-mediated mechanism. The Na-CDs demonstrated a 180 nm red-shift in emission, transitioning from 450 to 630 nm. The Na, B-CDs achieved blue-shifted, multicolor emission, progressing from orange to yellow and green under 30-s UV irradiation. Notably, the photochromic states spontaneously reverted to their initial configurations without external stimuli. These phenomena arise from photoinduced electron transfer between pristine CDs and light-generated anionic radicals. Leveraging these unique photochromic properties, we implemented reversible anti-counterfeiting systems and information encryption platforms. Furthermore, the photochromic CDs exhibit daylight-responsive UV detection capabilities and are functional in plant cell imaging, significantly expanding their potential applications in optoelectronic devices.**

Keywords: carbon dots, photochromic, photoinduced electron transfer, reversible, fluorescence

INTRODUCTION

The development of reversible, light-responsive materials has made significant strides in applications such as information storage, bioimaging, optical switches, and security devices [1–3]. Among these systems, photochromic materials are particularly promising for light-responsive applications [4–6]. Organic photochromic compounds exhibit reversible color transitions upon light irradiation, a phenomenon originating from molecular transformations where photoexcitation induces either electronic transitions or structural rearrangements, thereby altering optical properties. Representative systems include spiropyran, azobenzene, and diarylethene derivatives [7–9]. Zhu *et al.* [10] designed a sterically hindered ethene-bridged photochromic triad integrated with ferrocene and naphthalimide, achieving redox-gated photochromism and photoinduced electron transfer (PET)-modulated fluorescence switching through controlled electron transfer between ferrocene redox states and the chromophore. Zhou *et al.* [11] successfully achieved reversible photochromism of viologen derivatives in multiple solvents by introducing triethylamine (TEA) as an electron donor to form charge-transfer complexes, which effectively facilitated the PET process. Wang *et al.* [12] developed a dual-emitting luminescent hybrid film UPTES-SPn-Tb-hfa based on photochromic spiropyran and terbium (Tb) complexes. By utilizing the ring-closing (SP)/ring-opening (MC) isomerization of SP to achieve fluorescence resonance energy transfer (FRET), the film exhibits reversible dynamic luminescence under alternating UV and visible light irradiation. However, photochromic materials still face challenges such as insufficient photostability, slow response rates, and limited reversibility.

Carbon dots (CDs), a type of 0D luminescent carbon nanomaterial, have attracted significant attention due to their diverse physicochemical properties, biocompatibility, unique optical characteristics, low cost, and eco-friendliness [13,14]. By tuning their chemical structures and dopants, CDs can be engineered into a variety of fluorescent behaviors [15–18]. However , there are currently limited reports on the photochromic properties of carbon dots, and the underlying mechanisms have not been thoroughly investigated. Liu *et al.* [19] reported the development of smart photochromic nanocomposites by integrating CDs with titanium dioxide (TiO_2) porous films, which exhibit bidirectional photochromism (coloration or discoloration) under single-wavelength visible light irradiation. Fu *et al.* [20] synthesized photochromic CDs via a one-step solvent-free microwave-assisted method using naphthalene tetracarboxylic acid, urea, and boric acid ; these CDs exhibit reversible fluorescence color switching under UV light in amine solvents, and highlight their potential applications in UV detection and dynamic anticounterfeiting. Guo *et al.* [21] fabricated CDs-based materials with intrinsic photochromism, multi-stimulation-responsive afterglow (lifetime of 253 ms), and dynamic color regulation by embedding naphthalimide structures in CDs and using polyvinylpyrrolidone encapsulation. However, most reported photochromic CDs materials achieve only a single-color change with a relatively small emission range span, while their slow response and poor reversibility make them unsuitable for complex application scenarios.

Here, 1,4,5,8-naphthalenetetracarboxylic dianhydride (NTCDA) was used as a precursor, employing conventional hydrothermal synthesis to prepare photochromic CDs through

Key Laboratory for Biobased Materials and Energy of Ministry of Education/Guangdong Provincial Engineering Technology Research Center for Optical Agriculture, College of Materials and Energy, South China Agricultural University, Guangzhou 510642, China
* Corresponding author (email: tleibf@scau.edu.cn; thucf@scau.edu.cn)

Na and B co-doping, enabling the CDs solution to exhibit multicolor photochromism (Fig. 1a). The resulting CDs achieved rapid emission changes: Na-CDs transitioned from blue to red, while Na, B-CDs progressed from blue to red and then to green under UV irradiation, establishing multicolor photochromic behavior (Fig. 1b). We propose that this luminescence mechanism occurs because UV irradiation causes excitons to reach the excited state, while partial energy transfer to new energy levels induces photochromic phenomena (Fig. 1c). Notably, these photochromic CDs maintain dynamic color transitions when incorporated into PVA hydrogels, offering a viable pathway for secure data encryption and UV detection by utilizing this unique fluorescent property.

MATERIALS AND METHODS

Materials and measurement

Reagents including boric acid (BA), sodium carbonate (Na_2CO_3), 1,4,5,8-naphthalenetetracarboxylic dianhydride (NTCDA), polyvinyl alcohol (PVA, Type 1799), dimethyl sulfoxide (DMSO), polyethylene glycol (PEG), and *N*,*N*-dimethylformamide (DMF) were sourced from Aladdin and used without further purification. Deionized (DI) water was employed throughout the study.

Transmission electron microscopy (TEM) images were obtained on a JEOL JEM-F200. High-resolution transmission electron microscopy (HR-TEM) characterization was implemented on a 200 kV TEM microscope. X-ray photoelectron spectroscopy (XPS) measurements were performed on a Thermo Scientific K-Alpha. Fourier transform infrared (FT-IR) spectra were obtained on a Thermo Fisher. UV-visible absorption spectra were scanned using UV-2600i (Shimadzu). Photoluminescence spectra (PL) were obtained on an Edinburgh FLS 1000 fluorescence spectrophotometer equipped with a xenon arc lamp (Xe900) and a microsecond flash-lamp (μF900). Fluorescence lifetime curves of CDs in solution were determined using a steady-state fluorescence spectrometer (Edinburgh FLS1000, UK). Photographs were taken by an EOS 40D camera under ambient conditions. Electron spin resonance (ESR) signals were obtained on a Bruker EMXplus-6/1 spectrometer, and the samples were excited using a 365 nm UV lamp. A Nikon Ds-R2 Inverted Fluorescence Microscope takes photos of plant cells.

Density functional theory (DFT) calculations were carried out with the Gaussian 16 software. The B3LYP functional was

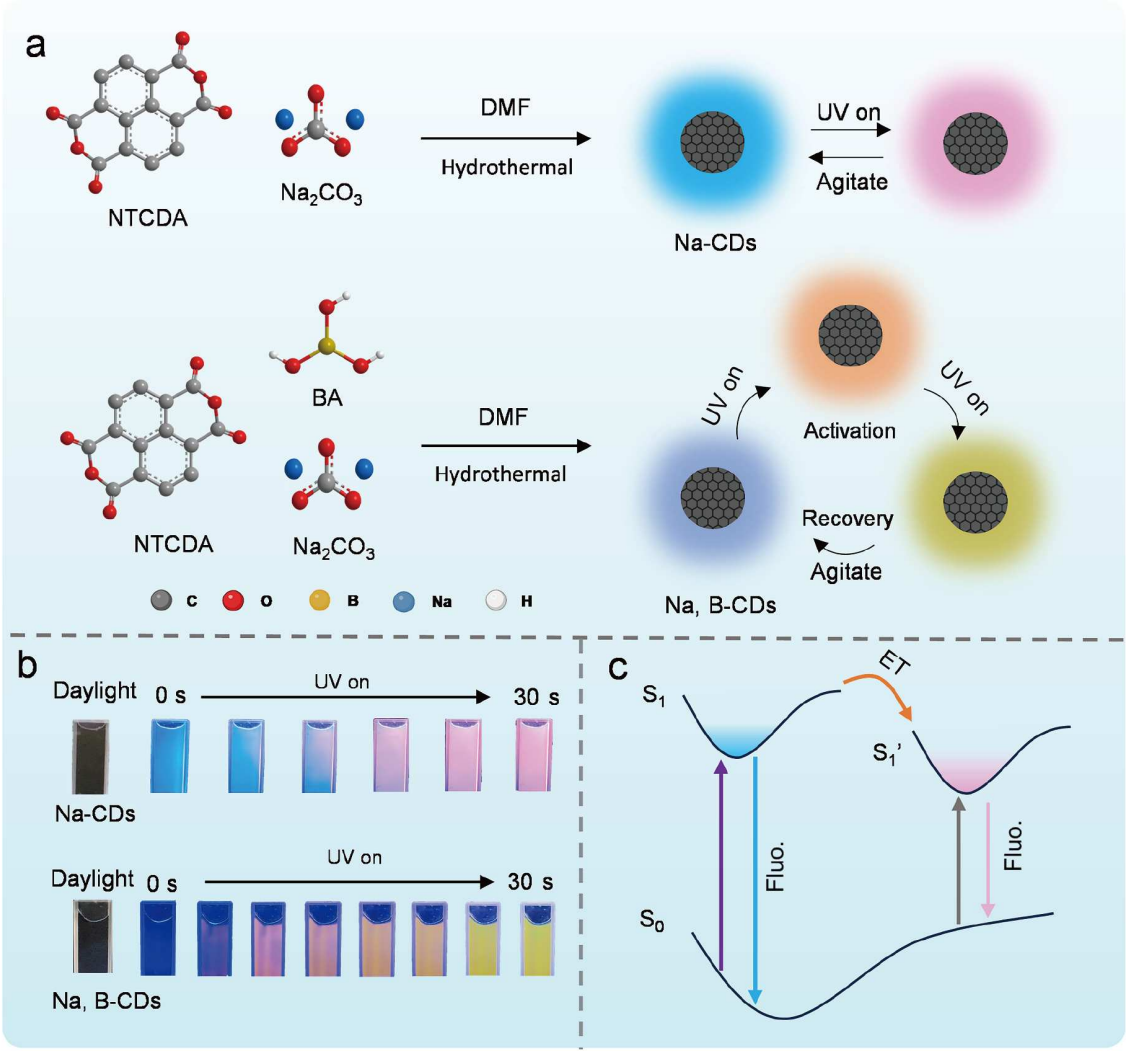

Figure 1 Stimulating photochromism in CDs. (a) Preparation of the photochromic CDs. (b) UV light stimulation of CDs in response to photochromic pictures. (c) Proposed mechanism for photochromic CDs.

adopted for all calculations in combination with the D3BJ dispersion correction. For geometry optimization and frequency analysis, the 6-31+G (d, p) basis set was utilized for all atoms. Single-point calculations were carried out at the M062X-D3/6-311+G (d, p) level. The Solvation Model Based on Density (SMD) implicit solvation model was applied to account for solvation effects during optimization and frequency calculations, with DMF chosen as the solvent. Frontier orbital analysis was conducted using the Multiwfn and VMD software packages.

Synthesis and preparation

Synthesis of the Na-carbon dots (Na-CDs)

First, 0.2 g of sodium carbonate and 0.2 g of NTCDA were added to the liner of a 100 mL autoclave. Then, 50 mL of DMF was introduced and stirred vigorously. Subsequently, the mixture was reacted at 200 °C for 6 h in an oven. After cooling, the resulting solution was filtered through a 0.22 μm organic filter membrane and dialyzed using a 500 Da dialysis bag for 4 h to obtain the Na-CDs.

Synthesis of the Na, B-CDs

1 g of BA and 0.2 g of sodium carbonate were added into the liner of a 100 mL reaction kettle; 50 mL of DMF was added and stirred vigorously. Then, 0.2 g of NTCDA was added into the reaction kettle and homogenized. The mixture was heated at 200 °C for 5 h in an oven. After the reaction, the solution was filtered through a 0.22 μm organic filter membrane, and the precipitate was collected. The precipitate was dissolved in 50 mL of deionized water, sonicated, and centrifuged at 10,000 r/min for 5 min to remove insoluble impurities, yielding Na, B-CDs.

Preparation of the CDs-PVA film

0.5 g PVA was mixed with 10 mL H_2O and 1 mL Na-CDs solution at 90 °C oil bath condensation reflux for 1 h, poured into the mold placed in a ventilated place air-drying static overnight, and then placed in an 80 °C oven drying.

Preparation of the CDs-PVA hydrogel

10 g PVA was dissolved in 90 g H_2O at 85 °C to form a PVA aqueous solution; separately, 10 g PVA was dissolved in 90 g DMSO at 85 °C to form a PVA-DMSO solution. Then, 3 g of PVA aqueous solution and 7 g of PVA-DMSO solution were mixed thoroughly, followed by the addition of 1 mL of Na-CDs and further mixing. The mixture was centrifuged at 4000 r/min for 2 min to remove bubbles. The resulting CDs-PVA hydrogels were poured into a mold and stored at 4 °C overnight.

Preparation of the CDs ink

2 g of PEG_{800} was melted by heating and mixed with 1 mL of Na-CDs by ultrasonication, and left to stand overnight, and then added the appropriate amount into the stamp with a dropper and left to stand for 15 min; PEG_{200} was mixed with Na, B-CDs by ultrasonication according to the ratio of 1:1.

Na, B-CDs in plant cell imaging

Mung bean seeds were soaked in deionized water overnight and subsequently transferred to a dark room for incubation for 5 days, and observed daily for growth. The mung bean sprout stems were placed in CDs solution for overnight incubation when they grew to about 10 cm. The cultured mung bean sprout stems were taken, and thin cross-section samples were prepared by the freehand sectioning method.

RESULTS AND DISCUSSION

Preparation and characterization of the photochromic CDs

The morphologies of Na-CDs and Na, B-CDs were characterized using transmission electron microscopy (TEM). Both CDs exhibited good dispersion with quasi-spherical shapes and showed similar particle sizes, averaging 2.36 nm for Na-CDs and 2.40 nm for Na, B-CDs. The high-resolution TEM (HRTEM) images revealed well-resolved lattice fringes having a spacing of 0.21 nm, indicating a graphite-like core structure (Fig. 2a, b) [22]. Fourier transform infrared spectroscopy (FTIR), and X-ray photoelectron spectroscopy (XPS) were used to analyze the surface functional groups of Na-CDs and Na, B-CDs (Fig. 2c, d). Like the precursor, synthesized CDs (NTCDA) exhibited vibrational signals of about 3450 cm^{-1}, indicating the presence of –OH groups, suggesting hydrophilicity of the CDs. Peaks at 1630 and 1380 cm^{-1} this is due to stretching vibrations of C=O and C–N [23]. The characteristic absorption at 1187 and 952 cm^{-1} is due to the bending vibration of B–O–H and the telescopic vibration of B–C [24,25]. The integrated XPS spectra (Fig. 2d) of the CDs showed the presence of C, N, O and Na, in addition to which, the B element was also present in the Na, B-CDs. The high-resolution XPS spectra of C 1s, N 1s, O 1s, and Na 1s for Na-CDs and Na, B-CDs were examined. In the Na-CDs C 1s XPS spectrum, distinct peaks were observed: C–C/C=C (284.8 eV), with a peak area percentage of 89.73% after convolution fitting; C–O/C–N (286.2 eV), with a peak area percentage of 3.07% after convolution fitting; and C=O (288.4 eV); C–N (399.3 eV) and N–H (400.1 eV) in N 1s XPS spectrum; C=O (531.2 eV) and C–O/O–H (532.9 eV) in the O 1s XPS spectra, and Na Auger (535.6 eV); in the Na 1s XPS spectra, the binding energy of Na was 1071.3 eV (Fig. 2e, f; Fig. S1). Significant peaks can be seen in Na, B-CDs XPS spectra: C–C/C=C (284.8 eV) with a convolved fitted peak area percentage of 69.65%, C–O/C–N (286.4 eV) with a convolved fitted peak area percentage of 11.50% and C=O (288.0 eV); N 1s XPS spectra for C–N (399.0 eV) and N–H (400.1 eV); C=O (531.3 eV) and C–O/O–H (532.6 eV) in the O 1s XPS spectra, and Na Auger (536.4 eV); in the Na 1s XPS spectra, the binding energy of Na was 1071.8 eV; in the B 1s XPS spectra, the binding energy of B–O (192.3 eV) and B–C (192.5 eV) (Fig. 2g–i; Fig. S2) [24]. The area ratio of C–C/C=O convolution peaks in Na, B-CDs decreased compared to that of Na-CDs, while the percentage area of C–O/C–N convolution peaks increased, indicating that the doping with electron-deficient B elements results in a reduction of the structure of the sp^2 conjugated domain of the CDs [26,27].

Photophysical property investigations

The prepared Na-CDs and Na, B-CDs exhibit similar photophysical properties. To elucidate their photophysical processes, transient absorption spectroscopy and transient fluorescence spectroscopy were conducted on both CDs. Na-CDs in DMF solution and Na, B-CDs in aqueous solution at room temperature and without activation showed an absorption peak at 210 nm. This indicates the presence of aromatic C–C structure in the carbon nucleus and a strong n–π* absorption band roughly at 340 nm. With the increase of UV irradiation time

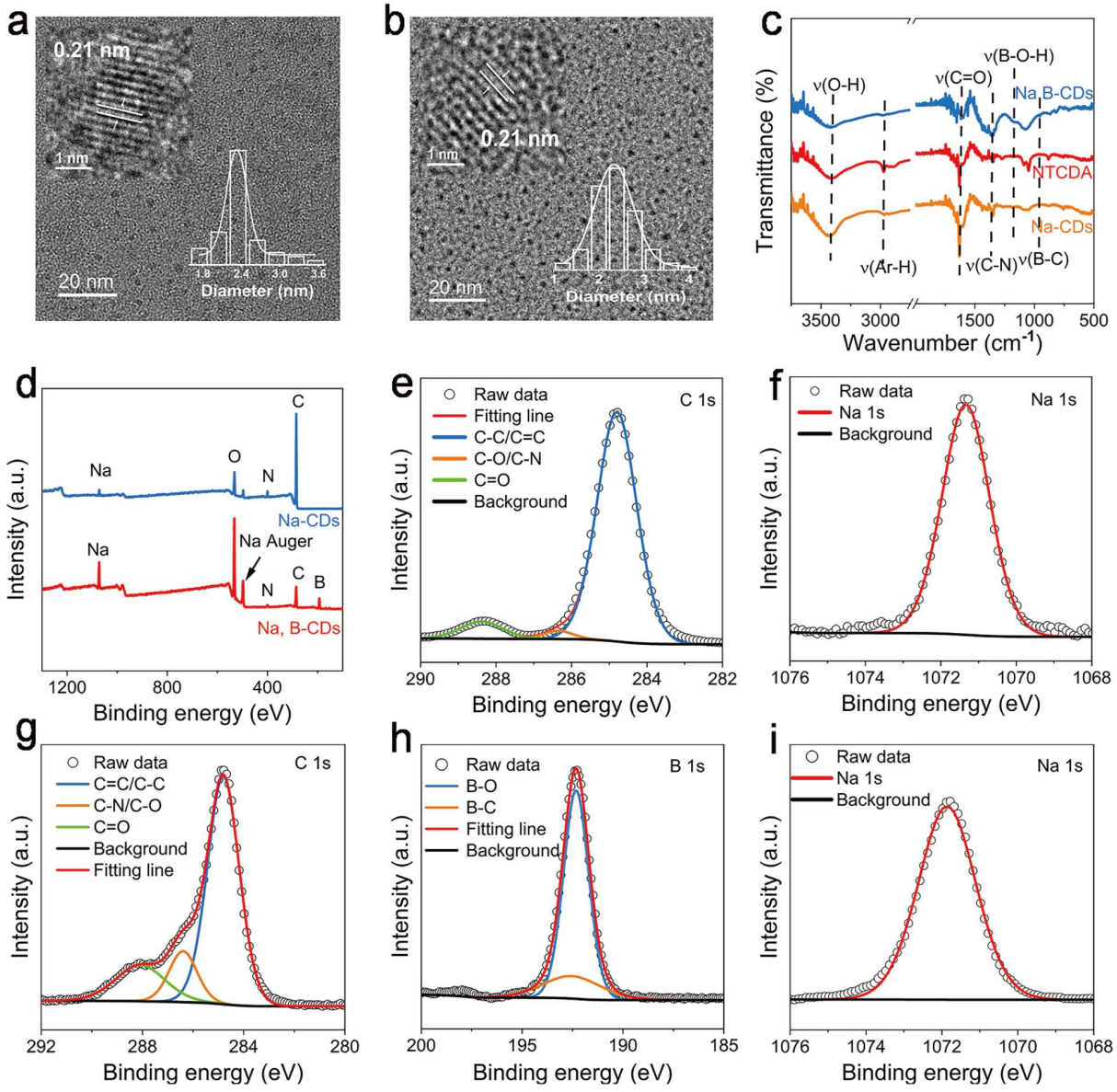

Figure 2 Structure characterization of photochromic CDs. TEM image of the CDs with the size distribution diagram and HRTEM images of the (a) Na-CDs and (b) Na, B-CDs (inset). (c) FTIR spectra of the Na-CDs, NTCDA, and Na, B-CDs. (d) XPS of Na-CDs and Na, B-CDs. High-resolution XPS spectra of (e) C 1s and (f) Na 1s of the Na-CDs. High-resolution XPS spectra of (g) C 1s, (h) B 1s, and (i) Na 1s of the Na, B-CDs.

(within 30 s), it can be found that the absorption bands of the two kinds of CDs between 450–650 nm gradually enhanced. The appearance color of the Na-CDs solution gradually became darker, while the appearance color of Na, B-CDs solution did not change significantly (Fig. 3a, Figs S3–S5). The newly generated absorption bands indicate the production of new substances under the excitation of UV light, which is attributed to the PET behavior of the surface of the CDs due to the generation of anionic radicals from UV irradiation.

In addition, the photochromic behavior of Na-CDs and Na, B-CDs under UV irradiation was investigated. Na-CDs fluoresced at 450, 525 and 420 nm under 365 nm excitation. Under continuous irradiation at 365 nm, the fluorescence intensity of Na-CDs at 450 and 525 nm was gradually increased at the beginning, reflecting a photoactivation phenomenon [28,29]. Subsequently, the fluorescence intensity gradually decreased and the fluorescence peak position shifted to 630 nm. With photochromism, the fluorescence color also changed from blue to red, and an obvious redshift occurred (Fig. 3b, Video S1). The main emission peak of Na, B-CDs was at 400 nm, and a peak at about 600 nm appeared within 2 s of UV irradiation, followed by a gradual blueshift of the peak to 520 nm. With photochromism, the fluorescence color changed from blue-violet to orange and then gradually to yellow, and finally blue-shifted to green, and the change was more rapid (Fig. 3c, Video S2). There is an overlap between the fluorescence spectrum after UV activation and the newly generated absorption peaks in the UV-visible absorption spectrum after photoactivation, which provides the feasibility for CDs to realize the PET process (Fig. 3d) [30,31]. It was interesting to note that in addition to the 365 nm excitation that produces the photochromic process, 395 nm excitation also produces a different color change for these two CDs. The Na-

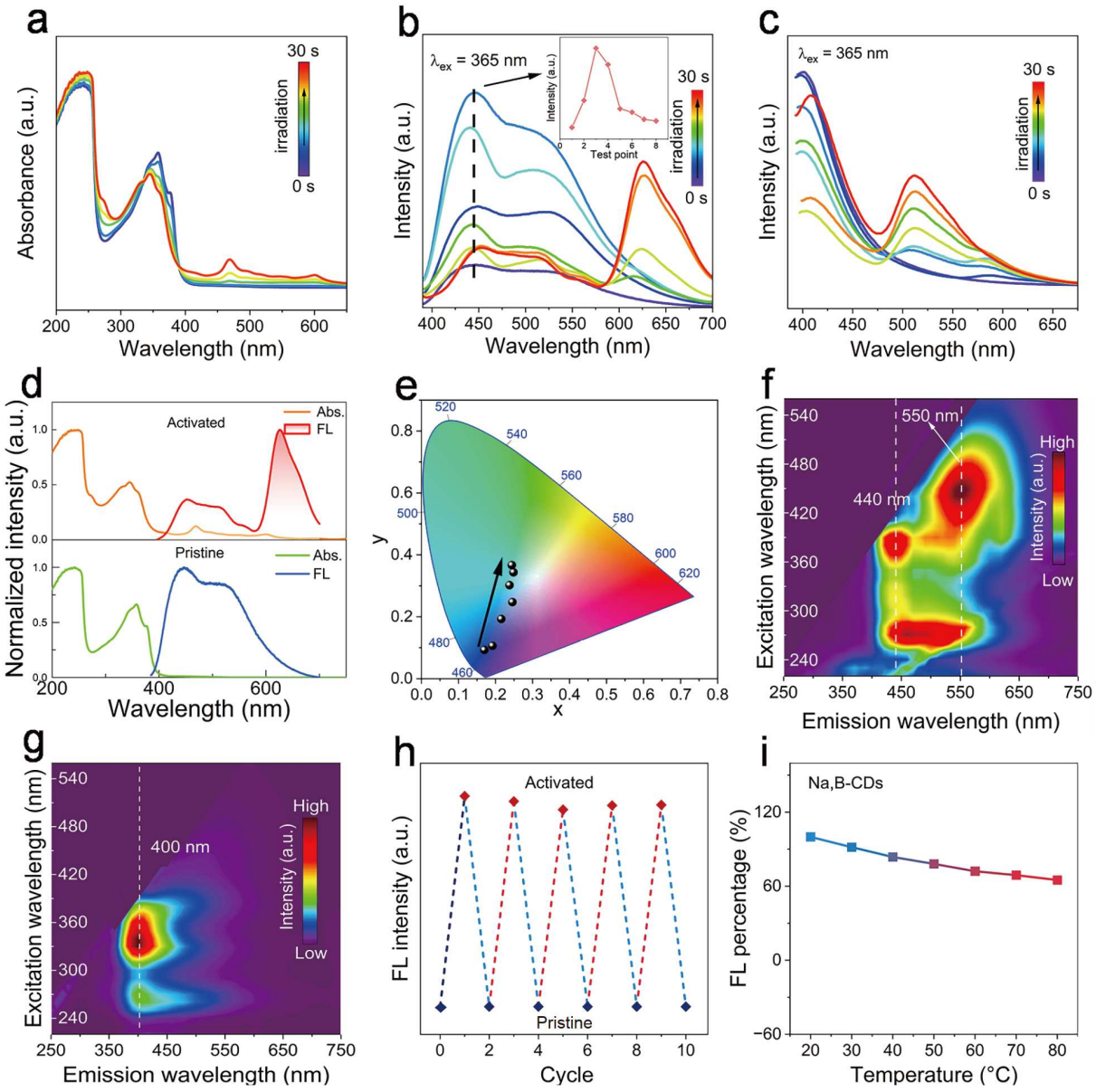

Figure 3 Photophysical properties of the CDs before (pristine) and after (activated) the photoirradiation. *In situ* absorption spectra of (a) Na-CDs under 365 nm irradiation for different times. Under 365 nm activation, transient fluorescence spectra of (b) Na-CDs and (c) Na, B-CDs. (d) Photophysical properties of Na-CDs *in situ* and after activation, absorption (blue), fluorescence spectra (red). (e) CIE coordinates of Na, B-CDs after irradiation for different times. Excitation-emission mapping of the photoactivated (f) Na-CDs and (g) Na, B-CDs. (h) Reversibility of the activated and deactivated PL. (i) Temperature profiles of Na, B-CDs with respect to fluorescence correlation.

CDs changed from green to red under 395 nm excitation, and the Na, B-CDs changed from blue to orange (Fig. S6). Further analysis by means of the 1931 International Commission on Illumination (CIE) chromaticity diagram to examine the fluorescence changes of Na-CDs and Na, B-CDs before and after UV irradiation showed that the fluorescence color changes characterized by the CIE spectra agree with the visual observations (Fig. 3e, Fig. S7).

We found a meaningful phenomenon. To explore the effect of doping with other metal elements, we synthesized K-CDs, Rb-CDs, and Mg-CDs with similar structures to NTCDA. By studying the transient fluorescence spectra under UV light irradiation, it is interesting to note that the photochromic color changes vary after light excitation. However, all the CDs exhibited three emission peaks at 430, 530 and 630 nm. This suggests that ionic doping mainly modifies the non-radiative recombination paths through surface modification, thus modulating the fluorescence intensity. It indicates that ion doping mainly modifies the non-radiative recombination paths of CDs through surface modifications (e.g., passivating defects, modulating charge transfer) to modulate the fluorescence intensity, whereas the surface state energy levels are not significantly altered, and thus the positions of the emission peaks remain stable (Fig. S8) [32–34]. Furthermore, excitation-emission mapping shows that Na-CDs could be excited in the 240–530 nm range, exhibiting excitation-dependent behavior due to abundant surface states (Fig. 3f) [35]. Na, B-CDs can be excited in the 240–390 nm range, with excitation wavelength-

independent PL emission peaking at 400 nm (Fig. 3g). It should also be noted that activated CDs can be inactivated by shaking or standing and then reactivated again by UV light with excellent reversibility (Fig. 3h, Fig. S9). To evaluate the thermal stability of Na, B-CDs, the fluorescence intensity of the CDs was measured by placing the CDs at different temperatures. Na, B-CDs could still retain 65% of their fluorescence intensity at a high temperature of 80 °C, and Na-CDs can also maintain around 55%, indicating that both CDs have good stability and can remain stable in extreme environments (Fig. 3i, Fig. S10).

Mechanism investigations

To further investigate the luminescence mechanism of photochromic CDs, we performed electron paramagnetic resonance (EPR) tests. The EPR signals were significantly enhanced upon UV irradiation, and the strong resonance signal with a g-factor of 2.003 indicated the generation of associated free radicals, which corresponds to the previous conclusions (Fig. 4a, d) [36,37]. Therefore, the original CDs can be activated by light and then transfer energy to the newly generated radicals through PET [38,39]. The fluorescence lifetime of Na-CDs decreased from 2.5 to 1.49 ns after UV irradiation (λ_{em} = 450 nm), while the fluorescence lifetime at 630 nm only increased from 5.6 to 5.87 ns (Fig. 4b, c). Na, B-CDs showed similar properties: the fluorescence lifetime at 520 nm increased from 5.46 to 8.21 ns, while that at 400 nm decreased (Fig. 4e, f). This provides additional evidence for the dynamic nature of fluorescence changes. It has been reported that the reaction of 1,4,5,8-naphthalenetetracarboxylic acid dianhydride in DMF yields a naphthalene diimide structure [40]. Therefore, we hypothesized that CDs containing naphthalene diimines are generated during the reaction process. Subsequently, density-functional theory (DFT) studies were performed to verify our conjecture regarding the luminescence mechanism [22,41]. The DFT results indicate that

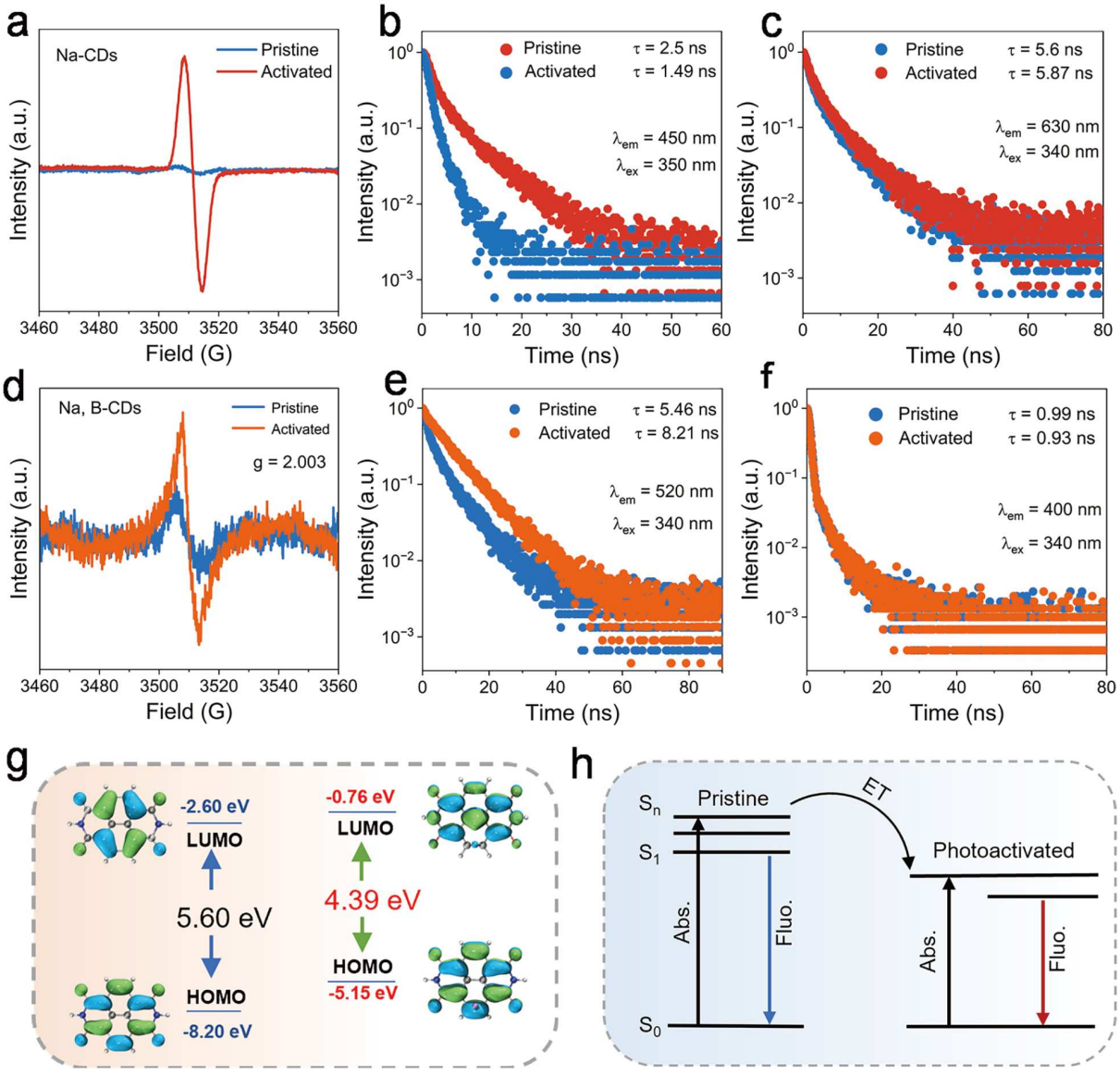

Figure 4 Photochromic mechanisms. (a) EPR spectra of Na-CDs. Fluorescence at (b) 450 nm (c) 630 nm decay profiles of the pristine (blue line) and photoactivated (orange line) Na-CDs. (d) EPR spectra of Na, B-CDs. Fluorescence at (e) 520 nm (f) 400 nm decay profiles of the pristine (yellow line) and photoactivated (red line) Na, B-CDs. (g) DFT calculated the energy levels of HOMO-LUMO. (h) Proposed mechanism for the reversible photochromic behavior.

doping Na into CDs introduces additional electrons into the electronic system of CDs, thereby elevating the HOMO orbital energy. Consequently, the energy of LUMO orbitals is also elevated due to the redistribution of electron cloud density, ultimately reducing the HOMO-LUMO energy gap and causing a redshift in the color of CDs (Fig. 4g) [42,43].

Based on the above analysis, we propose a possible mechanism for photochromic CDs (Fig. 4h). Under UV light excitation, the original Na-CDs are excited to the S_1 state via light absorption. The S_1 exciton can decay back to the S_0 state to produce fluorescence. Under continuous UV irradiation, photoactivation generates corresponding radicals, leading to photochromism. The transition of these radicals accelerates PET between different energy levels of Na-CDs and causes a transition to a new emission level, resulting in the appearance of new absorption peaks and thus achieving a change in fluorescence color [44]. The photochromic mechanism of Na, B-CDs is similar to that of Na-CDs. UV irradiation induces radical formation on the surface, leading to the occurrence of PET and a change in fluorescence color.

Cryptographic anti-counterfeiting applications, UV detectors, and plant cell imaging

The unique photochromic properties of CDs were harnessed for multilevel information security, encryption/decryption, and UV detection in combination with polyethylene glycol (PEG) and

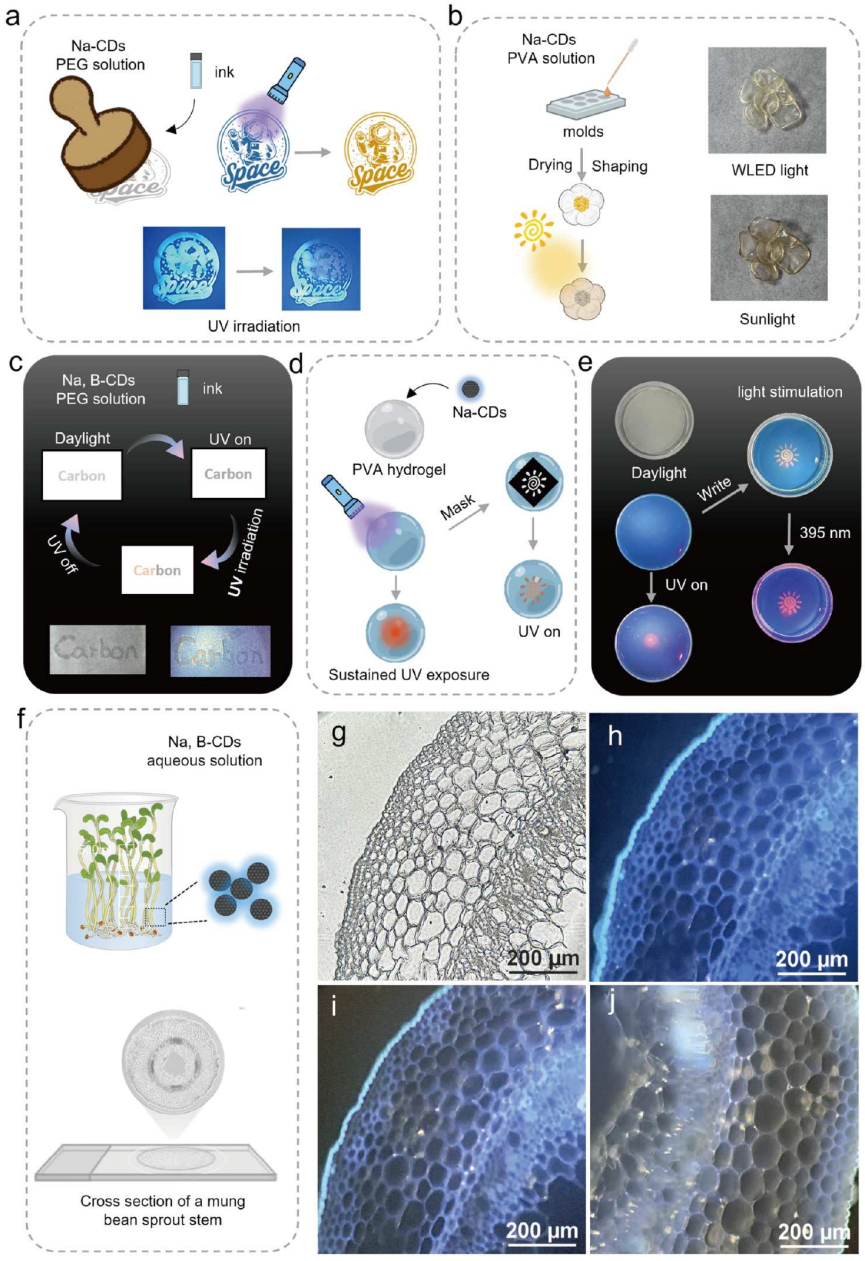

Figure 5 Applications in data anti-counterfeiting, information encryption, and UV detection. Schematic diagram of the application process of (a) dynamic information security, (b) UV detection, (c) information encryption ink, and (d, e) data writing and erasure. (f) Cross-sectional imaging of mung bean sprout stems. (g) Photograph of plant cells under bright field. (h) Photograph of plant cells under dark field (UV on). (i) Photograph of plant cells irradiated with 365 nm for 10 s in a dark field. (j) Photograph of plant cells irradiated with 365 nm for 20 s in a dark field.

polyvinyl alcohol (PVA). Na-CDs were employed as ink for stamps, with patterns printed on non-fluorescent paper. Upon exposure to 365 nm UV light for 10 s, the patterns gradually shifted from blue to brown in the strongly irradiated areas, while the remaining regions retained their initial color (Fig. 5a). Since the Na-CDs-PVA membranes have a sensitive detection effect on UV light, and the Na-CDs-PVA membranes gradually changed from light yellow to dark brown under UV irradiation, we prepared UV detection patterns with UV response (Fig. 5b). When the film was placed under the sun, the film rapidly changed to dark brown, and after the sun went down, the Na-CDs-PVA film gradually returned to the initial state, and the change was reversible. Subsequently, the Na-CDs-PVA film was made into a flower, and the edges of the flower darkened when exposed to sunlight (UV index = 6) and returned to the original state after the sun went down, which demonstrated that our detection device is suitable for UV detection.

Additionally, the unique photochromic properties of CDs were exploited, employing an aqueous solution of Na, B-CDs as a cryptographic security ink for monochrome printing (Fig. 5c). By using Na, B-CDs ink and PEG_{200} to write the "Carbon" message on paper, the "Carbon" message was displayed under UV light, and when the message is exposed to UV light for a long time, the CDs are activated by light, and their appartent color changes to orange, and finally the "Car" message was decrypted through the photochromic effect. Masked patterns on 25 cm^2 of Na-CDs PVA hydrogels were used as writing instruments, in which the designed patterns were printed by UV irradiation for 10 s. The photoactivated photochromic patterns are very stable to UV excitation, can be easily deactivated by standing, and are highly reversible for multiple cycles (Fig. 5d, e). By using an inverted fluorescence microscope to observe the cross-sections of mung bean sprouts, when the plant cells were irradiated with 365 nm fluorescence in the dark field, the cells showed blue fluorescence, and the outline of the cells could be clearly seen; the color of the cells gradually changed to orange as the irradiation time increased. These images show that Na, B-CDs can be fluorescently imaged in plants and are accompanied by color changes (Fig. 5f–j).

CONCLUSIONS

In summary, we have successfully synthesized CDs exhibiting fluorescent photochromism, which can be photoactivated to generate corresponding free radicals under external UV light stimulation. Na-CDs can be transformed from blue to red under 365 nm excitation, while Na, B-CDs exhibit blue-orange-green color change. By further combining with PVA, PEG, and other polymers, these materials have been realized for applications in information security, data encryption/decryption, UV detection, and plant cell imaging. This work provides a new approach for developing light-responsive, color-changing CDs and offers a design strategy for exploring multicolor color-changing materials.

Received 9 June 2025; accepted 10 July 2025; published online 12 August 2025

1 Lin Z, Yang J, Zeng Q, *et al.* Deep blue photoluminescence and optical gain from sodium-doped carbon dots. J Lumin, 2022, 246: 118856
2 Zhang J, Zou Q, Tian H. Photochromic materials: more than meets the eye. Adv Mater, 2013, 25: 378–399
3 Julià-López A, Hernando J, Ruiz-Molina D, *et al.* Temperature-controlled switchable photochromism in solid materials. Angew Chem Int Ed, 2016, 55: 15044–15048
4 Xiao Y, Shen M, Li J, *et al.* Thermally activated photochromism: realizing temperature-gated triphenylethylene photochromic materials. Adv Funct Mater, 2024, 34: 2312930
5 Thaggard GC, Kankanamalage BKPM, Park KC, *et al.* Switching from molecules to functional materials: breakthroughs in photochromism with MOFs. Adv Mater, 2024, 2410067
6 Wu NM, Ng M, Yam VW. Photochromic benzo[*b*]phosphole alkynylgold(I) complexes with mechanochromic property to serve as multistimuli-responsive materials. Angew Chem Int Ed, 2019, 58: 3027–3031
7 Sekar R, Basavegowda N, Jena S, *et al.* Recent developments in heteroatom/metal-doped carbon dot-based image-guided photodynamic therapy for cancer. Pharmaceutics, 2022, 14: 1869
8 Khandelwal H, Schenning APHJ, Debije MG. Infrared regulating smart window based on organic materials. Adv Energy Mater, 2017, 7: 1602209
9 Li XT, Li MJ, Tian YL, *et al.* A reversible photochromic covalent organic framework. Nat Commun, 2024, 15: 8484
10 Cai Y, Gao Y, Luo Q, *et al.* Ferrocene-grafted photochromic triads based on a sterically hindered ethene bridge: redox-switchable fluorescence and gated photochromism. Adv Opt Mater, 2016, 4: 1410–1416
11 Guo Z, Su Y, Zong H, *et al.* A universal strategy for reversible photochromism of viologen derivatives in solutions. Adv Opt Mater, 2024, 12: 2401791
12 Bai Z, Guo L, Zhao D, *et al.* Photochromic spiropyran-based dual-emitting luminescent hybrid films for dynamic information anticounterfeiting. ACS Appl Mater Interfaces, 2024, 16: 44018–44025
13 Miao S, Liang K, Zhu J, *et al.* Hetero-atom-doped carbon dots: doping strategies, properties and applications. Nano Today, 2020, 33: 100879
14 Liu H, Zhong X, Pan Q, *et al.* A review of carbon dots in synthesis strategy. Coord Chem Rev, 2024, 498: 215468
15 Zhang C, Zheng K, Ye X, *et al.* Effects of nonmetallic heteroatoms doping on the catalytic performance of carbon materials. Chem Eng Sci, 2025, 304: 120980
16 K. Algethami F, Abdelhamid HN. Heteroatoms-doped carbon dots as dual probes for heavy metal detection. Talanta, 2024, 273: 125893
17 Zhang X, Hou L, Samorì P. Coupling carbon nanomaterials with photochromic molecules for the generation of optically responsive materials. Nat Commun, 2016, 7: 11118
18 Fu Q, Sun S, Lu K, *et al.* Boron-doped carbon dots: doping strategies, performance effects, and applications. Chin Chem Lett, 2024, 35: 109136
19 Wu J, Fu S, Zhang X, *et al.* Bidirectional photochromism via anchoring of carbon dots to TiO_2 porous films. ACS Appl Mater Interfaces, 2020, 12: 6262–6267
20 Zhang K, Fu Q, Sun S, *et al.* Photoluminescent multicolor carbon dots for UV detection and dynamic anticounterfeiting. ACS Appl Mater Interfaces, 2024, 16: 52833–52841
21 Guo Z, Bian Y, Zhang L, *et al.* Multi-stimuli-responsive carbon dots with intrinsic photochromism and *in situ* radical afterglow. Adv Mater, 2024, 36: 2409361
22 Sun J, Liu Y, Han Y, *et al.* Enabling controllable time-dependent phosphorescence in carbonized polymer dots based on chromophore excited triplet energy level modulation by ionic bonding. Angew Chem Int Ed, 2025, 64: e202415042
23 Ran Z, Jia H, Zhong Z, *et al.* Time-dependent room-temperature afterglow of carbon dots constructed by trap-induced multiemission centers. Nano Lett, 2025, 25: 6993–7002
24 Liu Y, Li W, Wu P, *et al.* Hydrothermal synthesis of nitrogen and boron co-doped carbon quantum dots for application in acetone and dopamine sensors and multicolor cellular imaging. Sens Actuat B-Chem, 2019, 281: 34–43
25 Hao H, Wang M, Cao Y, *et al.* Boron-doped engineering for carbon quantum dots-based memristors with controllable memristance stability. Small Methods, 2024, 8: 2301454
26 Tomskaya AE, Prosvirin IP, Egorova MN, *et al.* Structural and optical

properties of N-doped and B-doped carbon dots. J Struct Chem, 2020, 61: 818–825
27 Liu L, Lu Y, Wang S, *et al*. B, N stabilization effect on multicavity carbon microspheres for boosting durable and fast potassium-ion storage. J Colloid Interface Sci, 2022, 620: 24–34
28 Jiang L, Ding H, Lu S, *et al*. Photoactivated fluorescence enhancement in F, N-doped carbon dots with piezochromic behavior. Angew Chem Int Ed, 2020, 59: 9986–9991
29 Liao L, Qi J, Gao J, *et al*. Nitrogen-doped carbon quantum dots with photoactivation properties for ultraviolet ray detection. ACS Appl Mater Interfaces, 2024, 16: 42632–42640
30 Kudr J, Richtera L, Xhaxhiu K, *et al*. Carbon dots based FRET for the detection of DNA damage. Biosens Bioelectron, 2017, 92: 133–139
31 Wang Y, Zhou S, Pan S, *et al*. Color-tunable carbon dots with aggregation-induced emission constructed by FRET between surface luminescence centers. Adv Opt Mater, 2024, 12: 2301486
32 Yan Y, Zhang NN, Tauche LM, *et al*. Direct synthesis of a stable radical doped electrically conductive coordination polymer. Inorg Chem Front, 2022, 9: 5016–5023
33 Li X, Fu Y, Zhao S, *et al*. Metal ions-doped carbon dots: synthesis, properties, and applications. Chem Eng J, 2022, 430: 133101
34 Yu R, Ou M, Hou Q, *et al*. Metal and non-metal doped carbon dots: properties and applications. gxjzz, 2024, 5: 1
35 Xu Y, Wu M, Feng X, *et al*. Reduced carbon dots versus oxidized carbon dots: photo- and electrochemiluminescence investigations for selected applications. Chem Eur J, 2013, 19: 6282–6288
36 Li GP, Zhu H, Hao P, *et al*. The modulation effect of carboxylic acid ligands on the electron transfer photochromism of NDI-derived coordination polymers. Dalton Trans, 2021, 50: 15153–15161
37 Liu JJ, Wang ZJ, Xia SB, *et al*. Photochromic and photocontrolled luminescence properties of two metal-organic frameworks constructed from a naphthalene diimide derivative. Dyes Pigments, 2020, 172: 107856
38 Harvey CP, Tovar JD. Main-chain photochromic conducting polymers. Polym Chem, 2011, 2: 2699
39 Li L, Zeng JG, Zhang NN, *et al*. Naphthalene diimide-based crystalline hybrid photochromic materials: structural types, photochromic mechanism, and applications. Inorg Chem Front, 2025, 12: 11–38
40 Xiao P, Dumur F, Graff B, *et al*. Design of high performance photoinitiators at 385–405 nm: search around the naphthalene scaffold. Macromolecules, 2014, 47: 973–978
41 Sun J, Liu Y, Han Y, *et al*. Enabling controllable time-dependent phosphorescence in carbonized polymer dots based on chromophore excited triplet energy level modulation by ionic bonding. Angew Chem Int Ed, 2025, 64: e202415042
42 Xiong T, Cen W, Zhang Y, *et al*. Bridging the g-C_3N_4 interlayers for enhanced photocatalysis. ACS Catal, 2016, 6: 2462–2472
43 Jiang J, Cao S, Hu C, *et al*. A comparison study of alkali metal-doped g-C_3N_4 for visible-light photocatalytic hydrogen evolution. Chin J Catal, 2017, 38: 1981–1989
44 You MH, Li MH, Li HH, *et al*. The impact of metal cations on the photochemical properties of hybrid heterostructures with infinite alkaline-earth metal oxide clusters. Dalton Trans, 2019, 48: 17381–17387

Acknowledgement This work was supported by the National Natural Science Foundation of China (12274144 and 52472160) and the Natural Science Foundation of Guangdong Province (2023A1515012003 and 2025A1515010658).

Author contributions Cao J was responsible for synthesis and characterization and drafted the initial manuscript. Huang E, Zhong Z, and Jiang T characterized the properties of CDs. Li W, Zhang H, and Zhang X provided academic advice. Lei B and Hu C revised the initial manuscript, provided academic advice, and obtained funding. All authors participated in the overall discussion.

Conflict of interest The authors declare that they have no conflict of interest.

Supplementary information Supplementary materials are available in the online version of the paper.

Jueran Cao is a master's student at the School of Materials and Energy, South China Agricultural University, where her research focuses on the photochromic properties of fluorescent carbon dots.

Chaofan Hu is currently an associate professor at the School of Materials and Energy, South China Agricultural University. His research group focuses on the photoluminescence properties of carbon nanomaterials, including fluorescent carbon dots, graphene quantum dots, and polymer dots. They also explore the applications of these materials in bioimaging.

Bingfu Lei is currently a professor at the School of Materials and Energy, South China Agricultural University. His research group focuses on designing and synthesizing inorganic non-metallic materials and organic/inorganic hybrid materials. They also analyze the optical and electrical properties of rare-earth functional materials and conduct applied basic research.

光电子转移诱导的碳点双模式光致变色发光

曹珏然, 黄恩临, 钟紫婷, 江霆杰, 张浩然, 李唯, 张学杰, 胡超凡*, 雷炳富*

摘要 在功能材料中整合光致变色和光致发光面临着实现宽光谱颜色调制和快速响应的严峻挑战. 在此, 我们开发了掺钠和钠/硼共掺杂碳点(CDs), 它们通过一种新的自由基介导机制表现出双模光致变色发光行为. 钠掺杂的CDs在 450到 630 nm的波长范围内实现了180 nm的红移发射, 而钠/硼共掺杂的CDs则实现了蓝移多色发射, 在30 s紫外辐照下从橙色逐渐过渡到黄色和绿色. 值得注意的是, 光致变色态在没有外部刺激的情况下会自发恢复到初始状态. 这些现象源于原始CDs与光产生的阴离子自由基之间的光诱导电子转移. 利用这些独特的光致变色特性, 我们实现了可逆防伪系统和信息加密平台. 此外, 光致变色CDs还具有日光响应紫外检测能力和植物细胞成像能力, 这大大拓展了光致变色CDs的应用前景.

